The Meteoritical Society

Meteoritics & Planetary Science 48, Nr 6, 1074–1090 (2013)
doi: 10.1111/maps.12133

Clasts in the CM2 carbonaceous chondrite Lonewolf Nunataks 94101: Evidence for aqueous alteration prior to complex mixing

Paula LINDGREN[1*], Martin R. LEE[1], Mahmood R. SOFE[1], and Michael E. ZOLENSKY[2]

[1]School of Geographical and Earth Sciences, University of Glasgow, Glasgow G12 8QQ, UK
[2]NASA Johnson Space Center, Mail Code KT, Houston, Texas 77058, USA
[*]Corresponding author. E-mail: paula.lindgren@glasgow.ac.uk

(Received 19 January 2012; revision accepted 21 April 2013)

Abstract–Clasts in the CM2 carbonaceous chondrite Lonewolf Nunataks (LON) 94101 have been characterized using scanning and transmission electron microscopy and electron microprobe analysis to determine their degrees of aqueous alteration, and the timing of alteration relative to incorporation of clasts into the host. The provenance of the clasts, and the mechanism by which they were incorporated and mixed with their host material are also considered. Results show that at least five distinct types of clasts occur in LON 94101, of which four have been aqueously altered to various degrees and one is largely anhydrous. The fact that they have had different alteration histories implies that the main part of aqueous activity occurred prior to the mixing and assimilation of the clasts with their host. Further, the presence of such a variety of clasts suggests complex mixing in a dynamic environment involving material from various sources. Two of the clasts, one containing approximately 46 vol% carbonate and the other featuring crystals of pyrrhotite up to approximately 1 mm in size, are examples of unusual lithologies and indicate concentration of chemical elements in discrete areas of the parent body(ies), possibly by flow of aqueous solutions.

INTRODUCTION

Background

Clasts of lithologies that are foreign to the host rock occur in all classes of meteorites, for example, in ureilites (Prinz et al. 1987; Brearley and Prinz 1992; Bischoff et al. 2010); HED achondrites (Reid et al. 1990; Brearley and Papike 1993; Zolensky et al. 1996); ordinary chondrites (Semenko et al. 2001, 2005; Nakashima et al. 2003); carbonaceous chondrites (Olsen et al. 1988; Bischoff et al. 1993; Endress et al. 1994; Greshake et al. 2002; Jogo et al. 2011); and in ungrouped meteorites, such as the Kaidun microbreccia (Zolensky et al. 1991; Zolensky and Ivanov 2003).

A recent survey of clast-bearing meteorites revealed the presence of several distinct classes of clasts, including in over 20 different carbonaceous chondrites (Zolensky et al. 2009). The most common types of clasts in carbonaceous chondrites are fine-grained hydrous clasts (Zolensky et al. 2009). These are dark, fine-grained, and heavily aqueously altered, and are often referred to as C1 or CI clasts (e.g., Grossman et al. 1988). Some studies have suggested that they are similar to hydrous micrometeorites (Gounelle et al. 2003, 2005), but they may also just represent new lithologies that have not been previously described. Fine-grained hydrous C1 or CI clasts have previously been described in, for example, CM chondrites (Olsen et al. 1988), CH chondrites (Greshake et al. 2002), and CR chondrites (Bischoff et al. 1993; Endress et al. 1994), but also in other meteorite groups, such as in ureilites (Brearley and Prinz 1992).

A better understanding of the mineralogy and provenance of clasts in meteorites is important for several reasons. For example, they can provide clues to the genesis and origin of some classes of meteorites, such as ureilites (Brearley and Prinz 1992); they may present an opportunity to study material not yet classified or available as separate meteorites, e.g., the Kaidun microbreccia (Zolensky et al. 1991; Zolensky and Ivanov 2003); and they can offer new information on thermal and/or aqueous alteration, mixing of material, and the relative timing between these processes

in the dynamic early history of the solar system (this study). Thermal and aqueous alteration, impact, and reaccretion are some of the earliest processes to have taken place in the asteroid belt (e.g., Petitat et al. 2011). The consequences of some of these processes are preserved in the carbonaceous chondrites, which are chemically the most primitive group of meteorites, but also the most highly aqueously altered (McSween 1979; Kallemeyn and Wasson 1981). Products of aqueous alteration are principally phyllosilicates, carbonates, hydrous sulfides, sulfates, and Fe-oxides (Zolensky and McSween 1988; Johnson and Prinz 1993; Zolensky et al. 1993; Brearley 2006; Lee and Ellen 2008). The mineralogy and composition of the secondary minerals, and the extent of preservation of primary phases, such as olivine, pyroxene, and Fe-Ni metal, varies with the degree of alteration (e.g., Zolensky et al. 1997; Rubin et al. 2007; Howard et al. 2009, 2011). The majority of aqueous alteration most likely occurred somewhere within asteroidal parent bodies, but the precise environment of alteration is currently poorly known (see reviews in Brearley 2003, 2006) and so analysis of clasts may provide new insights into these very early and important processes.

Aim of Study

The present paper is a detailed petrographic analysis of clasts in the CM2 carbonaceous chondrite Lonewolf Nunataks (LON) 94101. This is one of the clast-bearing meteorites that was included in the survey by Zolensky et al. (2009), who found it to have an exceptionally diverse population of clast lithologies. Here, our aim is to determine the relative timing of: (1) aqueous alteration of the clasts and the LON 94101 host, and (2) incorporation of the clasts into the LON 94101 host. In this study, we also consider the provenance of the clasts and the mechanism by which they were incorporated and mixed with their host carbonaceous chondrite.

MATERIAL AND METHODS

Samples

The CM2 carbonaceous chondrite LON 94101 was collected by US Antarctic Search for Meteorites program (ANSMET) in 1994 at Lonewolf Nunataks in Antarctica (81°20′ S, 152°50′ E). The total mass of this meteorite is 2804.6 g. Several broken pieces were recovered with abundant and extensive cracks and a moderate weathering grade (fracturing category C, weathering grade Be) (Antarctic Meteorite Newsletter (1995). Here, we have investigated six polished thin sections of LON 94101, which hereafter are referred to as (a) to (f). The sections are mounted on round glass slides (2.5 cm in diameter) and the sample sizes are approximately: 10 by 5 mm (a: LON 94101, 36), 8 by 7 mm (b: LON 94101, 33), 11 by 10 mm (c: LON 94101, LON), 15 by 12 mm (d: LON 94101, CARI1:), 13 by 12 mm (e: LON 94101, CARI2:), and 16 by 11 mm (f: LON 94101, CARI3:). Initial examination showed that only the thin sections a, b, and c contained clasts; hence, only these were used in further investigations.

Electron Microscopy

The thin sections with clasts were carbon coated and characterized via backscatter electron (BSE) imaging and qualitative energy dispersive (ED) X-ray mapping. This work used a Zeiss Sigma field-emission scanning electron microscope (SEM) operated at 20 keV/5 nA. The BSE imaging and ED X-ray mapping were undertaken using an Oxford Instruments INCA system together with an Oxford instruments X-MAX large area (80 mm^2) silicon-drift X-ray detector operated at a working distance of 8.5 mm. For a more detailed examination of the matrices of clasts, transmission electron microscopy (TEM) was performed on five focused ion beam (FIB) liftouts of matrix in five different types of clasts from two thin sections a and b. The foils were prepared using a FEI Nova 200 Dualbeam FIB instrument using 30 kV Ga^+ ions at a current ranging from 100 pA to 6 nA at different stages in foil milling. The foils were lifted out in situ using the procedure of Lee et al. (2003) and welded to the tines of a Cu support using both ion- and electron-deposited platinum. Diffraction contrast images and selected area electron diffraction (SAED) patterns were acquired from the foils using a FEI T20 transmission electron microscope (TEM) operated at 200 kV, whereas high-resolution images were obtained using a FEI TF20 TEM equipped with a field-emission gun (FEG). Further imaging and X-ray mapping of the FIB foils were carried out via low-voltage scanning transmission electron microscopy (LV-STEM) using the Zeiss Sigma SEM (further details in Lee and Smith 2006).

Raman Spectral Analysis

For identification of various mineral species in the clasts, Raman spectra were acquired using a Renishaw inVia Raman microscope with a 514 nm laser. Laser focusing on the sample was performed through a petrographic microscope fitted with a 100× objective. The spectra were accumulated in 30 increments with a measurement time of 2 s each, using only 10% of the

total laser power of 50 mW to avoid burning holes in the samples. The spot size was typically 1 μm, which was sufficiently small to only pick up spectra from one mineral grain. Calibration was made with respect to wave number using a Si standard. The collected Raman spectra were processed (curve fitted to determine the peak positions) using the Renishaw WIRE software. Electron microscopy and Raman spectral analysis were carried out at the University of Glasgow, UK.

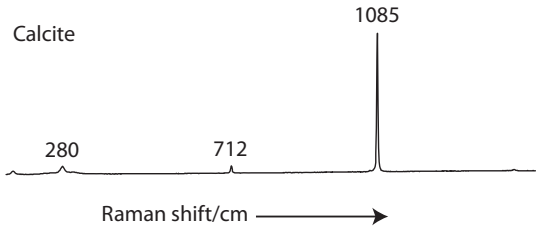

Fig. 1. Raman spectrum of calcite in the host LON 94101. The spectrum shows typical Raman bands for calcite at wave number shifts of approximately 280, 712, and 1085 cm^{-1}.

Electron Microprobe Analysis

Electron microprobe analyses of the clasts and their host meteorite were acquired using the CAMECA SX 100 electron probe microanalyzer (EPMA) at the University of Edinburgh, UK. The defocused beam size during analyses was 5 μm, which was small enough to target representative parts of the matrix (i.e., matrix with no major mineral inclusions or cracks or obvious rust veining). The accelerating voltage was set to 15 keV and the beam current was held at 10 nA for the major elements and 80 nA for minor and trace elements. Clast and host matrices were analyzed for Na, Mg, Al, Si, P, S, K, Ti, Cr, Mn, Fe, and Ni. The standards used were Na (jadeite), Mg (spinel), Al (spinel), Si (wollastonite), P (Durango apatite), S (pyrite), K (orthoclase), Ti (rutile), Cr (Cr metal), Mn (Mn metal), Fe (fayalite), and Ni (Ni metal). The maximum detection limits (in ppm) were as follows: Na (261), Mg (216), Al (305), Si (538), P (73), S (194), K (72), Ti (62), Cr (177), Mn (267), Fe (1157), and Ni (260). Fe-sulfides in one of the clasts were analyzed for Mg, Si, S, Cr, Mn, Fe, Ni, and Cu. The standards used were the same as above with addition of Cu (Cu metal) and the maximum detection limits (in ppm) were Mg (36), Si (90), S (959), Cr (176), Mn (282), Fe (2068), Ni (271), and Cu (427). Also, carbonates in one of the clasts were analyzed. Here, the beam current was set to 2 nA for the major elements and 40 nA for minor and trace elements. The carbonates were analyzed for Na, Mg, Al, Si, S, K, Ca, Cr, Mn, Fe, Ni, and Sr, using the same standards as above with the addition of Ca (calcite) and Sr (celestite). The maximum detection limits (in ppm) were Na (170), Mg (520), Al (125), Si (125), S (77), K (94), Ca (148), Cr (194), Mn (415), Fe (348), Ni (280), and Sr (372).

RESULTS

Initial examination of the six thin sections showed that only three contained clasts (a, b, and c), indicating that the distribution of clasts in LON 94101 is heterogenous. A total of 16 clasts were discovered in these three thin sections, and they can be divided into types 1–5 based on their textural, mineralogical, and chemical composition, and their degree of aqueous alteration (Table 1). The most common type of clast, comprising 12 out of the 16, is the so-called "CI-like clasts," or as termed hereafter: (1) "fine-grained hydrous clasts." Each of the other four clasts is different and here called (2) "fine-grained hydrous clast lacking clusters of Fe-oxide framboids," (3) "carbonate-rich clast," (4) "coarse sulfide-rich clast," and (5) "wavy sulfide-rich clast." The LON 94101 host and its various clasts are described in detail below.

The Host—LON 94101

LON 94101 is a CM2 carbonaceous chondrite and has been described in detail by Lindgren et al. (2011). It is composed of an optically dark hydrous matrix of finely crystalline phyllosilicates (Fe-Mg serpentines) with patches of sulfide/serpentine intergrowths, which are typical matrix constituents of CM2 chondrites (e.g., Brearley 2006). It contains approximately 7% chondrules, as determined by point counting, of which approximately 3% are mainly replaced by calcite and phyllosilicates, and the rest are largely unaltered and composed of olivine with minor pyroxene. Point counting was carried out systematically through the sample in the SEM, using images of the same scale and a centered cross hair to focus on the phase that was counted in each image. Furthermore, it contains approximately 3% calcite grains that are scattered throughout the matrix and these grains are often rimmed by sulfide/serpentine intergrowths. Raman spectral analysis was used to distinguish calcite from aragonite, and here it gave typical Raman bands for calcite at wave number shifts of approximately 280, 712, and 1085 cm^{-1} (Fig. 1), but rare aragonite also occurs in LON 94101 (Sofe et al. 2011). LON 94101 contains no dolomite or compositionally "complex" carbonates and >15% of the mafic silicates in the chondrules are altered; therefore, it belongs to the petrologic subtype CM2.2 according to the classification scheme of Rubin et al. (2007). Microprobe analyses show that the Fe concentration is higher, and the Mg

Table 1. The main characteristics of the five types of clasts found in three sections of LON 94101 (a, b, and c). The clasts are listed in order of decreasing degree of aqueous alteration (type 1 most altered and type 5 least altered).

Type	Name	Thin sections	Number found	Clast size (largest diameter)	Carbonate mineralogy	Matrix	Other characteristics	Classification
1	Fine-grained hydrous clasts	a, b, and c	12	~40–400 μm	Breunnerite and dolomite	Two varieties of ultrafine-grained phyllosilicates and ~100 nm sized grains of sulfides.	No anhydrous silicates. Contains clusters of iron oxide framboids.	C2.0 (C1) or CI?
2	Fine-grained hydrous clast lacking clusters of iron oxide framboids	a	1	~0.8 mm	Dolomite and calcite	Fine-grained phyllosilicates and ~200 nm sized iron-nickel sulfide grains.	No clusters of iron oxide framboids. Contains a few grains of olivine.	C2.1
3	Carbonate-rich clast	b	1	~2 mm	Siderite, breunnerite, and dolomite	Two varieties of fine-grained phyllosilicates and ~0.2 μm sized grains of iron-sulfides.	Consist of ~46% carbonates. Contains a few grains of olivine.	C2.1
4	Coarse sulfide-rich clast	b	1	~4 mm	Calcite	Three phyllosilicate phases: 1) a fine-grained phyllosilicate, 2) serpentine, and 3) chrysotile.	Olivine chondrule partially altered to calcite. Contains up to 1 mm sized laths of pyrrhotite.	C2.2–2.3
5	Wavy sulfide-rich clast	a	1	~1.2 mm	No carbonates	Matrix is mainly anhydrous, composed of olivine and some pyroxene. Possibly thin flakes of phyllosilicates at the rims of the olivine grains. Contains iron- and iron-nickel sulfides.	Largely composed of anhydrous silicates. Contains up to 100 μm sized elongated wavy pyrrhotites.	C3

concentration is lower, in the matrix of LON 94101 compared with the matrix of some of its included clasts (Table 2; Fig. 2). The microstructure of the calcite records at least three episodes of deformation of the LON 94101 parent body during and/or after aqueous alteration (Lindgren et al. 2011). This is seen in the calcite from e-twinning, microfaulting and subgrain rotation, and fragmentation and disruption of a vein.

Fine-Grained Hydrous Clasts

The 12 fine-grained hydrous clasts range in overall shape from irregular to rounded, but they all have rounded edges. Two of these clasts have disintegrated and appear "ghost-like" in the host. Their sizes range from approximately 40–400 μm, but most are approximately 200 μm in maximum size (Fig. 3a). They contain clusters of Fe-oxide framboids (Fig. 3b),

Table 2. Matrix compositions of four types of hydrous clasts and the host LON 94101 (wt%).

Name	Na_2O	MgO	Al_2O_3	SiO_2	P_2O_5	S	K_2O	TiO_2	Cr_2O_3	MnO	FeO	NiO	Total
Fine-grained hydrous clast-1	0.16	19.63	3.05	29.55	0.08	1.63	0.11	0.10	0.51	0.12	16.36	2.34	73.65
Fine-grained hydrous clast-2	0.15	18.51	5.40	39.76	0.07	1.36	0.17	0.12	0.40	0.10	13.09	2.75	81.87
	0.12	14.64	4.76	37.15	0.08	1.77	0.25	0.12	0.43	0.09	14.87	2.91	77.18
	0.26	22.03	3.41	37.01	0.08	2.02	0.18	0.14	0.45	0.11	15.14	3.05	83.88
	0.26	22.53	3.51	36.19	0.08	1.89	0.31	0.12	0.43	0.10	13.26	3.01	81.69
Fine-grained hydrous clast-3	0.60	24.15	2.65	38.18	0.07	1.20	0.14	0.06	0.38	0.07	10.65	1.04	79.18
Fine-grained hydrous clast-4	0.45	22.47	1.88	32.46	0.18	1.61	0.06	0.09	0.25	0.14	11.36	1.52	72.48
Fine-grained hydrous clast-5	0.94	18.54	2.00	31.31	0.13	3.26	0.16	0.12	0.46	0.16	15.11	2.29	74.48
Fine-grained hydrous clast-6	0.93	20.09	2.79	38.47	0.08	2.05	0.19	0.09	0.42	0.05	13.53	1.52	80.21
Fine-grained hydrous clast-7	0.79	23.56	2.81	39.69	0.02	2.47	0.15	0.07	0.51	0.11	12.36	1.68	84.24
Fine-grained hydrous clast-8	0.69	21.20	2.81	35.17	0.14	2.12	0.33	0.10	0.43	0.11	10.87	1.89	75.88
Fine-grained hydrous clast-9	0.84	18.10	1.82	35.09	0.08	1.21	0.18	0.12	0.32	0.17	13.22	2.50	73.66
Fine-grained hydrous clast-10	0.76	22.54	2.84	36.55	0.05	1.64	0.16	0.10	0.47	0.08	10.11	2.80	78.10
	0.67	23.69	2.79	38.05	0.05	1.00	0.18	0.07	0.45	0.06	9.47	2.37	78.87
Carbonate-rich clast	0.16	16.76	3.31	34.85	0.09	1.64	0.24	0.12	0.48	0.10	17.53	1.82	77.12
	0.14	14.02	2.96	31.41	0.09	1.63	0.17	0.12	0.47	0.09	20.26	1.74	73.10
	0.16	17.03	3.08	35.88	0.11	1.76	0.27	0.14	0.56	0.11	18.70	2.02	79.81
Fine-grained hydrous clast lacking framboids	0.40	17.68	3.29	28.39	0.28	3.56	0.15	0.09	0.18	0.22	27.64	1.06	82.95
	0.33	18.55	3.85	28.52	0.17	3.05	0.14	0.09	0.20	0.24	27.41	0.85	83.41
	0.30	17.40	4.21	29.09	0.15	2.67	0.11	0.10	0.20	0.23	28.34	0.96	83.75
Coarse sulfide-rich clast	0.23	17.60	2.65	29.67	0.02	0.35	0.06	0.09	0.52	0.25	24.81	0.23	76.47
	0.30	16.83	2.44	26.61	0.00	0.34	0.04	0.07	0.50	0.22	21.24	0.32	68.93
	0.50	16.64	2.52	27.25	0.01	0.73	0.05	0.09	0.42	0.26	27.10	0.44	76.02
	0.54	14.51	2.47	26.58	0.02	0.52	0.16	0.08	0.37	0.26	26.26	0.19	71.96
Matrix of host LON 94101	0.39	12.59	2.48	25.83	0.04	1.27	0.04	0.07	0.21	0.21	33.37	0.87	77.37
	0.41	14.76	2.37	24.13	0.05	4.06	0.06	0.07	0.31	0.21	28.40	1.41	76.25
	0.42	13.62	2.16	26.51	0.04	1.73	0.06	0.08	0.24	0.23	25.09	1.24	71.42

The analyses were acquired from ten different fine-grained hydrous clasts (1-10) and one clast of each of the four other types. Multiple analyses were acquired from fine-grained hydrous clast-2, each of the four other clast types, and from the LON 94101 matrix.

which are similar in appearance to magnetite framboids in many types of C chondrites, especially in CI and CM1 type material (Kerridge et al. 1979). It is therefore understandable that these types of clasts are often called "CI" or "CM1" clasts. They also contain sulfides along with dolomite and breunnerite (identified qualitatively by ED X-ray analyses), but lack chondrules and any other grains of anhydrous silicates. The matrix of these clasts is extremely fine-grained and EPMA data confirm that it has a lower Fe/Mg ratio than the host matrix

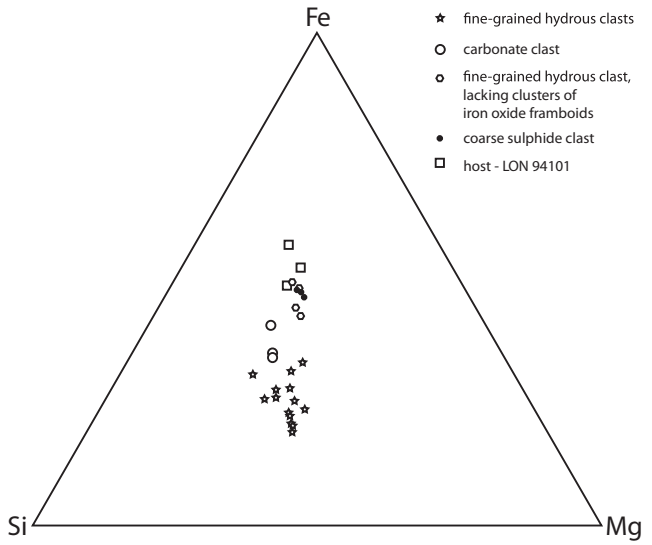

Fig. 2. Ternary diagram illustrating the atomic proportions of Si, Fe, and Mg in the matrices of four types of hydrous clasts and in the matrix of the host LON 94101. All the individual analyses are plotted (compare oxide data in Table 2).

(Table 1; Fig. 2). TEM diffraction contrast imaging reveals that the clast matrix is composed of two types of ultrafine-grained phyllosilicates, one wavy and slightly more coarsely crystalline and the other with a "sponge"-like texture (Fig. 3c). These phyllosilicates did not yield clear TEM SAED patterns or lattice fringes and so could not be unambiguously identified.

Fine-Grained Hydrous Clast Lacking Clusters of Fe-Oxide Framboids

One of the fine-grained hydrous clasts is distinct from the others in lacking clusters of Fe-oxide framboids, which are so abundant in the other fine-grained hydrous clasts. Also, this clast is larger, with more angular edges, and has a higher Fe/Mg ratio than the others (Table 2; Fig. 2). It is elongated and irregular in shape with a long axis of approximately 0.8 mm (Fig. 4a). This clast is composed of irregularly distributed approximately 10–20 μm sized grains of calcite and dolomite, and up to approximately 10 μm sized grains of sulfides and Fe-oxides (but no clusters of framboids) (Fig. 4b). It also contains a few grains of olivine with sizes of approximately 20–120 μm. EPMA data from the clast matrix show that it is compositionally similar to that of the host, but with a slightly lower concentration of Fe (Table 2; Fig. 2). TEM diffraction contrast images show the matrix to be composed of fine-grained, fibrous "fern"-like phyllosilicates (Fig. 4c) and equant sulfide grains approximately 200 nm in diameter (Fig. 4d). The phyllosilicates could not be identified from their SAED patterns or lattice fringe images, but LV-STEM X-ray

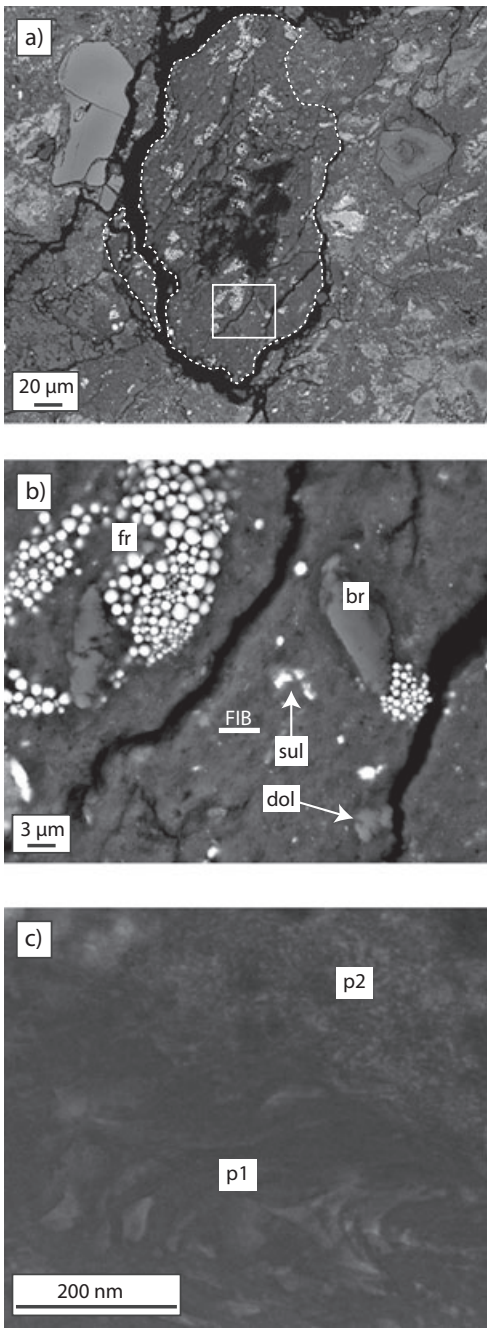

Fig. 3. a) SEM-BSE image of a fine-grained hydrous clast. The edge of the clast is outlined with a dashed white line. Note the ultrafine-grained matrix and the clusters of Fe-oxide framboids (white). The black areas are cracks and voids in the section filled with resin. b) Close-up SEM-BSE image of the area inside the white rectangle in (a) showing the mineralogy of this clast: breunnerite (br), Fe-oxide framboids (fr), sulfides (sul), and dolomite (dol), all embedded in an ultrafine-grained matrix. The white line (FIB) delineates the midplane of a foil that was cut and extracted from the clast using the FIB technique. c) A bright-field TEM diffraction contrast image showing the matrix to be composed of two types of ultrafine-grained phyllosilicates, p1 and p2, where p1 is wavy and slightly coarser than p2.

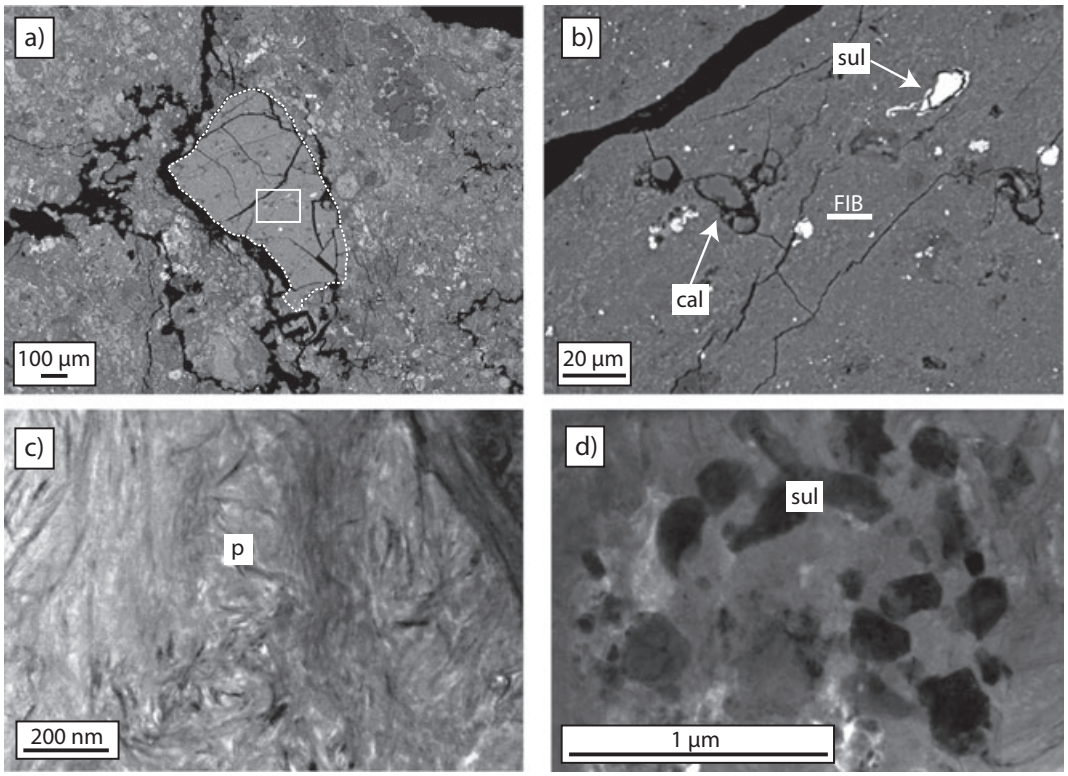

Fig. 4. a) SEM-BSE image of the fine-grained hydrous clast lacking clusters of Fe-oxide framboids (dashed white line). Note that this clast has a greater proportion of fine-grained matrix than its host meteorite. The black areas are cracks and voids in the section. b) Close-up SEM-BSE image of the area inside the white rectangle in (a) showing the mineralogy of this clast. It is composed of scattered approximately 10-20 μm sized grains of calcite and dolomite, calcite (cal) shown here, and up to approximately 10 μm sized grains of sulfides (sul) set in a fine-grained phyllosilicate matrix. This clast also contains Fe-oxides (but no clusters of framboids) and a few grains of olivine. The white line (FIB) delineates the midplane of a foil that was cut and extracted from the clast using the FIB technique. c) Bright-field diffraction contrast TEM image showing fine-grained fibrous phyllosilicates (p) of the clast matrix. d) Bright-field diffraction contrast TEM image showing 200 nm sized Fe,Ni-sulfides (sul) embedded in the matrix phyllosilicates.

mapping of the FIB foil shows that the sulfides are Ni-bearing and may be pentlandites.

Carbonate-Rich Clast

This clast is prominent in being composed of approximately 46 vol% carbonates (as determined via point counting); hence, it is termed "carbonate-rich clast." It appears to be slightly deformed with rounded edges and is elongated with a long axis of approximately 2 mm (Fig. 5a). The carbonates are set in a fine-grained matrix, which is revealed by TEM imaging and LV-STEM X-ray mapping to be composed of two phyllosilicate phases. The coarser phase consists of wavy flakes and yields lattice fringe spacings consistent with serpentine (0.7 nm). The other phase comprises a porous "sponge"-like material and 1 nm lattice fringe spacings that are suggestive of saponite (1 nm) (Fig. 5b). Grains of Fe-sulfides that range in size from approximately 20–200 nm are embedded in the matrix (Fig. 4b), and approximately 5 μm sized Fe-sulfide grains also occur in this clast (Fig. 5c). The matrix is depleted in Fe compared with the host, but is richer in Fe than the fine-grained hydrous clasts (Table 2; Fig. 2).

The carbonates that characterize this clast (Figs. 5c, d) are predominantly approximately 10–20 μm sized euhedral grains of siderite and ED X-ray mapping shows that they are zoned, with their cores having a higher Fe/Mg ratio than their narrow rims (Fig. 5d). The cores themselves are compositionally zoned, and many crystals have very fine-scale "dendritic" zoning interpenetrations with the rims. Of the ten microprobe analyses of "siderite" listed in Table 3, two are in fact breunnerite (i.e., Breunnerite_6 and _7). The low concentrations of Ca in these two datapoints show that they are not analyses of areas containing a mixture of siderite with dolomite and so it is likely that these are breunnerite forming narrow Mg-rich rims to the siderite grains. The edges of the siderite crystals are serrated and some have started to fragment along small "faults" that have submicrometer scale "throws." The carbonates

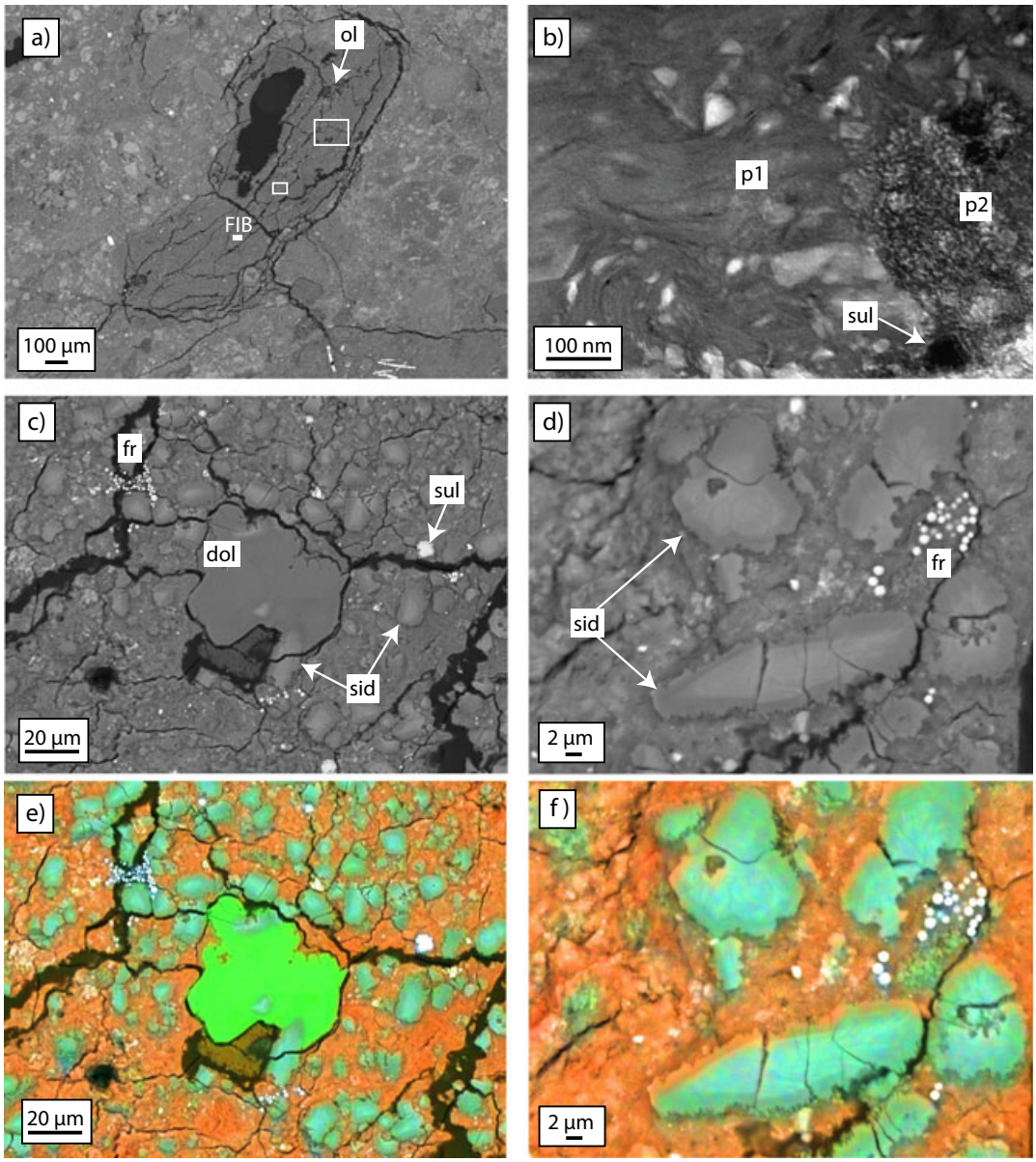

Fig. 5. a) SEM-BSE image of the carbonate-rich clast. The black areas are cracks and voids in the section. The white line (FIB) shows where a FIB foil was lifted out from the matrix. This clast contains a few grains of olivine (ol). b) A bright-field TEM diffraction contrast image showing the matrix to be composed of two types of fine-grained phyllosilicates, p1 and p2, where p1 forms wavy flakes and p2 is porous and "sponge" like. The matrix also contains abundant approximately 20-200 nm sized grains of sulfides (sul). c) Close-up SEM-BSE image of the area inside the larger white rectangle in (a) highlighting the mineralogy of this clast. It is composed of a large number of approximately 10 µm sized grains dominated by siderite (sid), a few approximately 50 µm sized grains of dolomite (dol), clusters of Fe-oxide framboids (fr), and sulfides (sul), all residing in the fine-grained phyllosilicate matrix. Note that a siderite-rich grain is intergrown with dolomite (sid, left arrow). d) Close-up SEM-BSE image of the area inside the smaller white rectangle showing the serrated edges of the siderite grains (sid) and Fe-oxide framboids (fr). Note the compositional zoning of the carbonate grains, whose centers are enriched in Fe (i.e., siderite) and rims enriched in Mg (i.e., breunnerite). To better display overall mineralogy, e) and f) are false-colored X-ray maps corresponding to c and d, respectively. The carbonates are represented by the green coloration: dark green for dolomite and light green for siderite. The red coloration denotes the Fe- and Mg-rich phyllosilicate matrix. White is Fe-oxides and Fe-sulfides.

of this clast include a few slightly larger approximately 40–60 µm diameter grains of Fe-rich calcian dolomite that are intergrown with the siderite-breunnerite crystals (Table 3; Fig. 5c). This clast also contains clusters of Fe-oxide framboids and a few grains of olivine. To highlight the mineralogy, Figs. 5e and 5f are

Table 3. Composition of ten siderite grains and six dolomite grains in the carbonate-rich clast (mol% carbonate).

Carbonate	$CaCO_3$	$MgCO_3$	$MnCO_3$	$FeCO_3$
Siderite_1	5.6	40.4	0.5	53.5
Siderite_2	5.2	42.9	0.7	51.1
Siderite_3	5.8	43.8	0.8	49.6
Siderite_4	7.3	32.5	0.6	59.7
Siderite_5	5.8	42.2	0.7	51.3
Breunnerite_6[a]	4.5	52.9	0.8	41.8
Breunnerite_7[a]	3.9	56.7	0.6	38.8
Siderite_8	4.6	36.4	2.1	56.9
Siderite_9	3.3	37.7	1.4	57.5
Siderite_10	4.1	42.4	1.2	52.4
Dolomite_1	51.8	41.5	0.5	6.1
Dolomite_2	55.8	38.7	0.1	5.4
Dolomite_3	56.3	38.4	0.4	4.9
Dolomite_4	51.7	40.9	0.3	7.1
Dolomite_5	55.7	38.9	0.4	5.0
Dolomite_6	53.7	40.2	0.4	5.8

[a]These analyses sample the breunnerite rims of the siderite grains.

corresponding false-colored X-ray maps of 5c and 5d, respectively. EPMA data are presented in Table 3 as mol% carbonate, and the full analyses are given in Appendix 1.

Coarse Sulfide-Rich Clast

The largest clast found is a hydrous approximately 4 mm maximum sized clast with up to approximately 1 mm long crystals of Fe-sulfides, which give a Raman spectrum of pyrrhotite, set in a fine-grained phyllosilicate matrix (Figs. 6a and 6b). This clast is called a "coarse sulfide-rich clast." The composition of the pyrrhotite was determined by EPMA (Table 4). It has approximately 0.6 wt% Ni (average of three analyses, Table 4). The pyrrhotite occurs as single crystals, which throughout the clast are elongate in a similar orientation, or in clusters (Fig. 6a). This clast also contains smaller grains of Fe-sulfides and Fe,Ni-sulfides, grains of calcite (distinguished from aragonite by Raman spectroscopy), and a chondrule composed of olivine that has been partially replaced by calcite. ED X-ray mapping and EPMA analyses of this clast show that the matrix is depleted in S and Ni, and to a lesser extent Fe, relative to the host (Table 2; Fig. 2). TEM images show that the matrix contains three phyllosilicate phases: (1) fine fibrous phyllosilicates with lattice fringe spacings consistent with serpentine (0.7 nm), (2) coarse tabular phyllosilicates that yield SAED patterns consistent with serpentine (Fig. 6c), and (3) hollow centered cylindrical chrysotile crystals approximately 20 nm in diameter (Fig. 3d). LV-STEM X-ray mapping shows that the coarser phyllosilicates are enriched in Fe compared to the finer phyllosilicates.

Table 4. Composition of three pyrrhotite grains in the coarse sulfide-rich clast (wt% element).

Sulfide	Mg	Si	S	Cr	Mn	Fe	Ni	Cu	Total
Pyrrh_1	0.00	0.06	39.3	0.00	0.00	60.4	0.53	0.02	100.3
Pyrrh_2	0.01	0.07	38.9	0.01	0.00	60.2	0.62	0.00	99.9
Pyrrh_3	0.01	0.08	38.9	0.00	0.01	60.2	0.64	0.00	99.9

Wavy Sulfide-Rich Clast

This is an irregular clast with a maximum size of approximately 1.2 mm composed mainly of mafic silicates: olivine and some pyroxene. It also contains wavy streaks of Fe-sulfides, all elongated in a similar orientation (Figs. 7a and 7b). The Fe-sulfides yield Raman spectra of pyrrhotite (Fig. 7b). X-ray mapping of the sulfides reveal that they contain some Ni, but they are too thin to be chemically analyzed by EPMA. ED X-ray analyses show that the olivines are richer in Mg than Fe and TEM SAED patterns yield solutions consistent with forsterite. Unfortunately, the porosity and fine grain size of this clast hindered acquisition of EPMA data from these mafic silicates, so their exact composition is unknown. The olivine grains are equant and up to 1 μm in diameter. The matrix of this clast is very porous and TEM images show the olivine grains to be embedded in an ultrafine material, which LV-STEM X-ray mapping shows to be resin-filled pores (amorphous material that contains carbon). There are, however, possibly some fine-grained fibrous phyllosilicates at the edges of the olivine grains (Fig. 7c). In addition to the wavy pyrrhotites, the clast contains approximately 0.2–0.4 μm sized equant pyrrhotite grains (Fig. 7d).

DISCUSSION

Relative Timing of Aqueous Alteration and Mixing

Aqueous alteration and mixing of material are amongst the earliest processes in the asteroid belt. The aqueous alteration most likely largely took place after material had accreted from the solar nebula and into parent bodies (e.g., see reviews in Brearley 2003, 2006), although it has also been suggested that aqueous alteration could have occurred prior to accretion and in a nebular setting (e.g., Bischoff 1998; Ciesla et al. 2003; Howard et al. 2011). One phase of mixing of material of course took place when the matter accreted from the solar nebula to parent bodies, but more complex mixing also occurred subsequently by processes such as impact disruption and reaccretion (e.g., Bunch and Chang 1980; Petitat et al. 2011) and/or via explosive degassing of water vapor followed by reassembly (e.g., Brearley 2006).

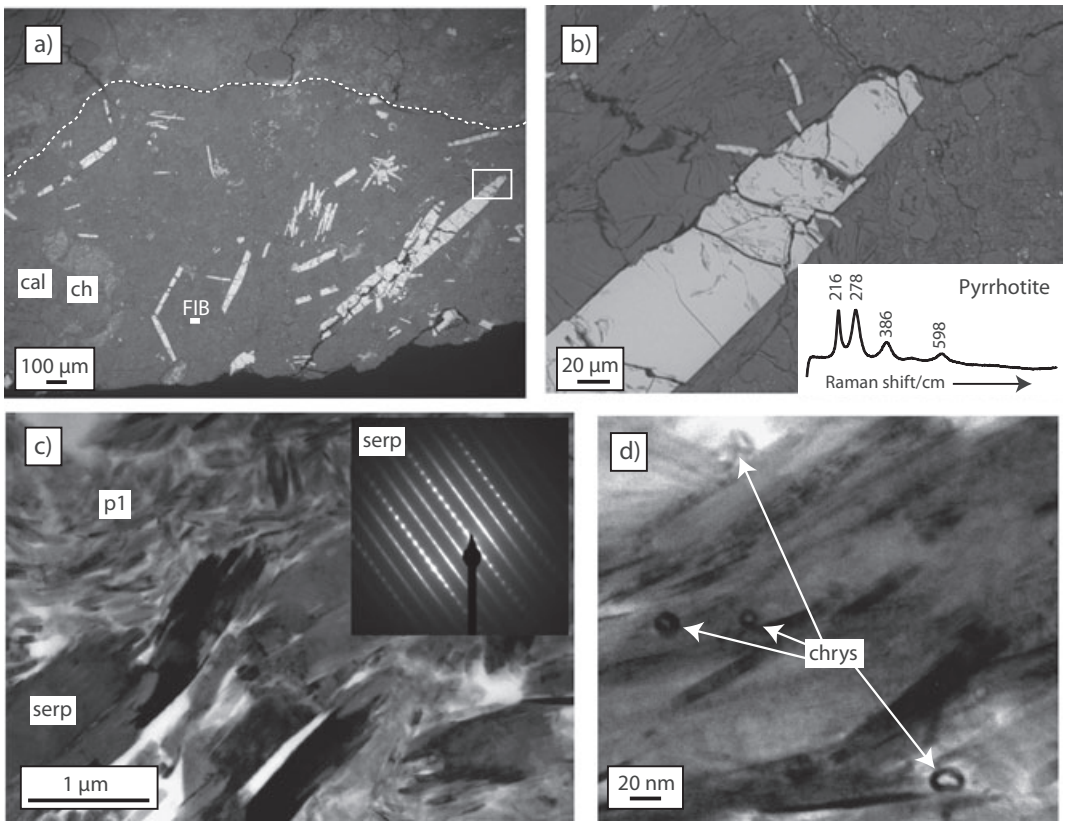

Fig. 6. a) SEM-BSE image of the coarse sulfide-rich clast. One edge of the clast is outlined with a dashed white line. Note the large, up to 1 mm long, crystals of pyrrhotite (bright elongated crystals), which occur singly, but elongated in a similar orientation, or as clusters. This clast contains one chondrule (ch) with olivine that has been partially replaced by calcite (cal). The white line (FIB) delineates the midplane of a foil that was cut and extracted from the clast using the FIB technique. b) Close-up SEM-BSE image of the area inside the white rectangle in (a) showing the edge of a pyrrhotite crystal and corresponding Raman spectra with typical Raman bands for pyrrhotite at wave number shifts of approximately 216, 278, 386, and 598 cm^{-1}. Note the smaller pyrrhotite laths that are extending out from the larger crystal. c) A bright-field TEM diffraction contrast image showing two types of phyllosilicates in the matrix; tabular serpentine (serp) with corresponding SAED pattern yielding a 0.7 nm spacing, and a finer fibrous variety of serpentine (p1) from which a good quality SAED pattern could not be acquired, but which yielded lattice fringe spacings of 0.7 nm (consistent with serpentine). d) A bright-field TEM diffraction contrast image showing 20 nm sized cylindrical chrysotile crystals (arrows, chrys) within the fibrous phyllosilicates.

Here, we want to establish the relative timing of aqueous alteration and the mixing of clasts with their host. To do this, we need to establish whether the clasts and the host have been aqueously altered to the same degree. If they have, aqueous alteration likely occurred after mixing, but if they are altered to different degrees, aqueous alteration took place prior to mixing. The host together with all the clasts, apart for the wavy sulfide-rich clast, contain a phyllosilicate matrix. Most previous studies of carbonaceous chondrite matrices have found that phyllosilicates are products of aqueous alteration on the parent body asteroids (e.g., Tomeoka 1990; Zolensky et al. 1993, 1997), although some phyllosilicates (Fe-cronstedtite) might have formed in the solar nebula prior to accretion (Howard et al. 2011). The degree of aqueous alteration in CM carbonaceous chondrites is determined via different classification schemes (e.g., Browning et al. 1996; Rubin et al. 2007; Howard et al. 2009, 2011). We cannot be certain that the clasts in LON 94101 are from the same source(s) as the CM carbonaceous chondrites, so it is not strictly accurate to adopt such a classification scheme for the clasts. However, for merely a comparison regarding the degree of aqueous alteration, we here use the classification scheme of Rubin et al. (2007), but we denote the clasts as, for example, C2.2 rather than C*M*2.2 etc. (Table 1). The host meteorite LON 94101 we know is a CM carbonaceous chondrite and it has been aqueously altered to a CM2.2 as it lacks dolomite or "complex" carbonates and 15–85% of the mafic silicates are altered. The clasts record alteration to various degrees: (1) The fine-grained hydrous clasts lack chondrules and anhydrous silicates; they are completely altered to secondary mineral phases. Hence, these are a subtype of

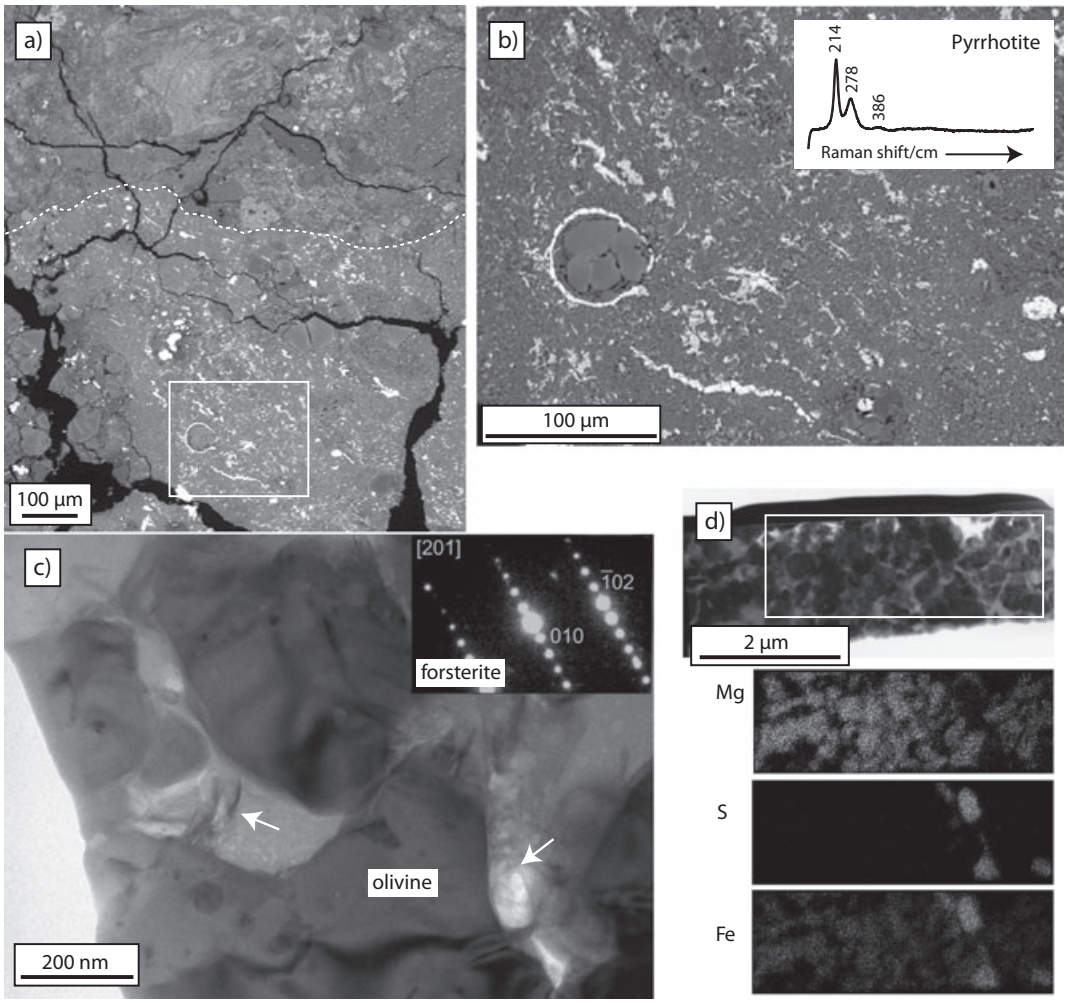

Fig. 7. a) SEM-BSE image of part of the wavy sulfide-rich clast. The edge of the clast is outlined with a dashed white line. Note the thin, wavy streaks of pyrrhotite (bright features), all elongated in a similar direction. This clast is largely anhydrous and, in addition to sulfides, is composed mainly of olivine and minor pyroxene. b) Close-up SEM-BSE image of the area inside the white rectangle showing the wavy pyrrhotites (bright) and a corresponding Raman spectrum with typical Raman bands for pyrrhotite, here at wave number shifts of approximately 214, 278, and 386 cm^{-1}. The matrix (gray) is largely composed of anhydrous silicates. c) Bright-field diffraction contrast TEM image of a foil extracted from the matrix of this clast using the FIB technique showing equant grains of olivine with a corresponding forsterite SAED pattern. The arrows point to possible fine-grained phyllosilicates at the edges of the olivine grains. d) Bright-field diffraction contrast TEM image of the foil and corresponding LV-STEM X-ray maps for Mg, S, and Fe. The X-ray maps were acquired of the area inside the white rectangle.

C2.0 (or C1). (2) In the fine-grained hydrous clast lacking clusters of Fe-oxide framboids, the carbonates comprise dolomite and calcite, which together with the occurrence of a few grains of olivine signify this clast as a C2.1. (3) The occurrence of "complex" carbonates and a few grains of olivine in the carbonate-rich clast fingerprint this clast also as a C2.1. (4) The coarse sulfide-rich clast is free of dolomite or "complex" carbonates and some mafic silicates have been preserved; hence, it can be classified as a C2.2–2.3. (5) The wavy sulfide-rich clast is significantly less altered than the other clasts described here, and is composed mainly of mafic silicates. Hence, it is close to a C3.

Thus, apart from the wavy sulfide-rich clast, all of the clasts in LON 94101 have a hydrous matrix and have been aqueously altered to various degrees. Three of the clasts (1–3) have been more highly aqueously altered than the host. These facts, together with the presence of an anhydrous clast, imply that the most severe period of aqueous alteration (at least in the specific region of the LON 94101 parent body that is represented by our sample meteorite) must have occurred prior to complex final mixing and incorporation of the clasts. Previous studies of other hydrous meteorites have also suggested that the presence of anhydrous clasts incorporated in a hydrous

host indicates that aqueous alteration occurred before final mixing (Zolensky and Ivanov 2003; MacPherson et al. 2009). Similarly, results from bulk oxygen isotopes of hydrous xenoliths in Murchison show that aqueous alteration of these xenoliths took place prior to incorporation with the Murchison host (Olsen et al. 1988). Furthermore, Lindgren et al. (2011) show that several episodes of deformation occurred on the LON 94101 parent body during and/or after aqueous alteration, which could be linked to the mixing of clasts with the host.

The Provenance of Clasts

1. The most common clasts are the fine-grained hydrous clasts. They are to some extent similar to CI and CM1 meteorites in that they completely lack mafic silicates, contain clusters of Fe-oxide framboids and Fe-Mg-Ca carbonates in a fine-grained phyllosilicate-rich matrix. Also, EPMA data show that their matrices are depleted in Fe and enriched in Mg compared with the host CM2. This is consistent with CI and CM material previously analyzed by Zolensky et al. (1993), and might be a reflection of the fact that CI material contains Fe-Mg serpentines and *saponite*, rather than predominantly Fe-Mg serpentine, including *cronstedtite* as in CM lithologies (Brearley 2006). With increasing degree of aqueous alteration, the phyllosilicate matrices of carbonaceous chondrites become progressively depleted in Fe and enriched in Mg, as a greater proportion of the original anhydrous silicates are replaced (McSween 1979; Hezel and Palme 2010). The fine-grained hydrous clasts could also be of CM1 type material, as the CMs do range from type 1 to 2 (Zolensky et al. 1997). Similar fine-grained hydrous clasts are also found in CH chondrites (Greshake et al. 2002), and in CR chondrites where they are interpreted to be xenoliths, i.e., of a different precursor material than their CR host (Endress et al. 1994). It is interesting to note that CI and CM1 carbonaceous chondrites are relatively rare as finds and falls here on the Earth, yet the fine-grained and hydrous CI-like clasts are quite common as clasts in other meteorites (e.g., Endress et al. 1994; Greshake et al. 2002). This could be because these phyllosilicate-rich rocks are extremely friable and so do not often survive the fall through the Earth's atmosphere as individual meteorites. Another explanation is that this CI-like material originated locally from the same parent as the host, and hence did not undergo a great deal of transportation and impact prior to incorporation. However, these clasts are often rounded, which implies that they have seen at least some degree of abrasion during transportation.
2. The fine-grained hydrous clast lacking clusters of Fe-oxide framboids is mineralogically different from, and slightly less aqueously altered than, the other fine-grained hydrous clasts. Hence, this clast probably came from a different source with a somewhat milder aqueous alteration history than the other fine-grained hydrous clasts.
3. The carbonate-rich clast contains approximately 46 vol% carbonates, which are present as siderite-breunnerite crystals and coarser calcian dolomites. The edges of the euhedral siderite crystals appear etched, which is possibly because phyllosilicates of the clast matrix have crystallized partly at the expense of breunnerite on the grain rims. It is significant that the replacement of breunnerite by phyllosilicates has also been described from QUE 93005 (CM2.1) (Lee et al. 2011) and so in both occurrences, crystallization of hydrous silicates continued after the carbonates. From the intergrowths of dolomite with siderite-breunnerite crystals, it is unclear whether the Fe-Mg carbonates crystallized before the Ca-Mg-Fe carbonates, or vice versa. Here, we suggest that the larger dolomite grain has grown to enclose euhedral siderite-breunnerite crystals (rather than the dolomite being partially replaced by siderite-breunnerite) so that the sequence of mineralization was in the order of dolomite-siderite-breunnerite-phyllosilicate. This is opposite to that of, for example, Tagish Lake, where phyllosilicates were replaced by carbonates (Zolensky et al. 2002). The composition of the dolomite in the carbonate-rich clast is approximately $Ca_{54.2}Mg_{39.8}Fe_{5.7}Mn_{0.4}CO_3$ (average of six analyses, Table 3). This is similar to dolomite in QUE 93005 (CM2) (Lee et al. 2011), and also to dolomite in ALH 84034 (Tyra et al. 2010), both of which are severely aqueously altered CMs. Furthermore, the $CaCO_3$ content of this dolomite is more similar to CM dolomite, being slightly higher in comparison to CI dolomite that typically has slightly substoichiometric $CaCO_3$ compositions (Endress and Bischoff 1996). Siderite is quite unusual in carbonaceous chondrites, but it occurs in the more aqueously altered ones, such as the CIs, e.g., Ivuna (Endress and Bischoff 1996) and in Tagish Lake (Zolensky et al. 2002). Also, Tyra et al. (2011a) describe siderite in the CR1 chondrite GRO 95577. The siderite composition in the carbonate-rich clast is $Ca_{5.2}Mg_{39.8}Fe_{54.0}Mn_{1.0}CO_3$ (average of eight analyses, Table 3) and this is actually more similar to the Tagish Lake than the Ivuna siderite; the Ivuna siderite contains much more $CaCO_3$

(approximately 15 mol%) (Zolensky et al. 2002). The carbonate-rich clast is not completely aqueously altered because it contains a few grains of olivine. This is similar to: (1) some carbonate-rich lithologies in Tagish Lake where olivine is replaced by carbonates (Zolensky et al. 2002), and (2) replacement of silicates by carbonates in CMs (e.g., Tyra et al. 2011b). However, the very large proportion of carbonates in this clast makes it unusual compared with the classified CIs and CMs. One possibility is that the carbonate-rich clast originates from so-called "asteroidal caliche" hypothetical carbonate-enriched deposits on asteroids that could have originated by leaching followed by reprecipitation and accumulation of carbonates (Zolensky et al. 1997).

4. The coarse sulfide-rich clast is also unusual in that it contains very large euhedral crystals of pyrrhotite. Acicular pyrrhotite crystals are also common to CM1 lithology clasts in the Kaidun microbreccia (Zolensky and Ivanov 2003). Sulfide laths also occur in the CR chondrites LAP 02342 (Wasson and Rubin 2009) and in Acfer 059 (Endress et al. 1994). However, the Kaidun pyrrhotites are only approximately 80 μm long, the sulfide laths in LAP 02342 have a maximum length of approximately 110 μm, and the sulfides in Acfer 059 are approximately 100 μm, which are all much smaller than the approximately 1 mm pyrrhotites in the coarse sulfide-rich clast. ED X-ray mapping and microprobe analyses of this clast show that its matrix has considerably lower concentrations of S and Ni than the LON 94101 host, and the other clast types, which is most likely due to leaching of these elements from the matrix during crystallization of the pyrrhotite crystals. The common orientation of most of the pyrrhotite crystals suggests that they crystallized under uniaxial lithostatic pressure at some depth within the parent body; notably Lee and Ellen (2008) described acicular aragonite crystals in Murray (CM2) that also shared a common orientation, again suggesting crystallization under uniaxial and static pressure. One explanation for the unusual size of the pyrrhotites is that they formed during a period when the region of the parent body from which the clast was derived was soaked in a highly reducing aqueous fluid; hence, giving the possibility of S and Ni to migrate frequently from the matrix and crystallize out to form the coarse sulfides. The size of these crystals suggests that saturation states were relatively low and crystallization occurred over an extended period of time. At approximately 0.6 wt%, the Ni content of the clast pyrrhotite is lower than that of CI chondrite pyrrhotites, where it is on average approximately 1 wt% (Bullock et al. 2005). These compositional differences may not be significant, or could suggest a non-CI parent body for this clast.
5. The wavy sulfide-rich clast differs from all the other clasts in that it is largely anhydrous. This clast is composed mainly of equant olivine grains, implying that these are not pseudomorphs after phyllosilicate grains, i.e., it is not former hydrous material that has been thermally metamorphosed (Huss et al. 2006). However, the presence of elongated wavy Fe-sulfides (pyrrhotite) shows that it has been exposed to some aqueous alteration, although it is significantly less altered than the other clasts, which all have a completely or near-completely hydrous matrix. Similar textures to the wavy Fe-sulfides have been reported surrounding anhydrous silicate grains in CMs, and are interpreted as late-stage aqueous reactions (Browning et al. 2000). This texture could also be a result of a shock remobilization of sulfides, although there is no other direct evidence of impact features. If this clast was to be classified according to Rubin et al. (2007), it would be close to a hypothetical CM3 as it is largely anhydrous. The main component of the clast has a forsteritic olivine composition, and so has the unique carbonaceous chondrite Acfer 094 (Newton et al. 1995; Greshake 1997), which has previously been suggested to be a CM3 carbonaceous chondrite (Bischoff and Geiger 1994). However, the olivine compositions of, for example, the CV3 chondrites range widely between both forsteritic and fayalitic (Krot et al. 1995); hence, this clast could also have, for example, a CV3 origin.

The various clasts cannot be definitively linked to known meteorite groups, but the wide variety of clasts that are present in LON 94101 indicates that this is material that came together from multiple sources. The clasts could have accumulated from a wider region of the asteroid belt, or they could be samples of different regions of the same parent body which have witnessed different alteration histories. In the clasts, we see features that are unusual in individual meteorites, i.e., the carbonate-rich clast and the coarse sulfide-rich clast. These characteristics may indicate some degree of fluid movement, and, in particular, concentration of ions in discrete areas of the parent body(ies).

Mechanisms of Mixing

Most (or all) CM carbonaceous chondrites are breccias (Bischoff and Schultz 2004; Bischoff et al. 2006), where the brecciation took place via explosive degassing of water vapor (e.g., Brearley 2006) and/or via impacts (e.g., Bunch and Chang 1980; Petitat et al.

2011). Most of these CM breccias, including LON 94101, are composed of a host matrix with a range of clast inclusions distributed heterogeneously throughout the host. Thus, these are matrix-supported breccias in contrast to, for example, Kaidun, which is composed of a much greater clast content. The clasts in LON 94101 are derived from a wide variety of sources, which have accreted to their host. Compaction (and possibly some heating) must have occurred after accretion of the clasts to "weld" the different materials together within the LON 94101 host. The clasts themselves must also have been compacted and lithified to some extent before incorporation, or they would not have survived. However, the clasts were likely to have been quite soft when incorporated as they were extensively aqueously altered, and composed largely of ductile ultrafine-grained phyllosilicates. The rounded edges of the fine-grained hydrous clasts could imply transportation and abrasion prior to incorporation, but could also be a result of that they were ductile when they were assimilated to the LON 94101 host. The elongation and slightly deformed shapes of both the fine-grained hydrous clasts and the carbonate-rich clast, imply that further compaction occurred after the clasts were included.

The presence of several distinct types of clasts in LON 94101 indicates a complex mixing in a dynamic environment and involving material from various sources. A diverse array of clasts that experienced different degrees of aqueous alteration is also reported, e.g., in the matrix of Murray (Rubin and Wasson 1986). The mixing could have taken place in shallow crustal levels of an asteroid during impacts of foreign bodies. The clasts could be derived from these foreign bodies with contrasting initial composition and history, or they could originate from different lithologies of the same parent body, mixed together via the impacts. There is no evidence of brecciation or disruption of chondrules in the host LON 94101, but evidence from calcite microstructures does show that it has experienced impact processing (Lindgren et al. 2011). Different CM chondrites from the same parent asteroid may differ in their degree of aqueous alteration due to, e.g., that they were shocked to different extents (Rubin 2012).

CONCLUSIONS

At least five distinctly different types of clasts occur in LON 94101. Four types have been aqueously altered to various degrees and one is largely anhydrous. This shows that the major part of aqueous alteration happened prior to the mixing and compaction of the clasts with their host. The occurrence of several distinct clasts in LON 94101 implies a complex mixing in a dynamic environment involving material from various sources. The mixing could have taken place via repeated impacts, and the clasts could be derived from a wide region of the asteroid belt, or they could be samples of different parts of the same parent body, but with different aqueous alteration histories. The carbonate-rich clast and the coarse sulfide-rich clast are examples of clasts with features that are unusual in individual meteorites. These indicate fluid movement and concentration of elements in discrete areas of the parent body(ies).

Acknowledgments—We are grateful to the Meteorite Working Group for loan of the thin sections. We thank Peter Chung, Brian Miller, and Colin How at the University of Glasgow, and Chris Hayward at the University of Edinburgh for skilled technical support, and Science and Technology Facilities Council (STFC) for funding. MEZ was supported by the NASA Cosmochemistry Program.

Editorial Handling—Dr. Adrian Brearley

REFERENCES

Antarctic Meteorite Newsletter 18 (2), August 1995, Houston, TX: NASA Johnson Space Center.

Bischoff A. 1998. Aqueous alteration of carbonaceous chondrites: Evidence for preaccretionary alteration—A review. *Meteoritics & Planetary Science* 33:1113–1122.

Bischoff A. and Geiger T. 1994. The unique carbonaceous chondrite Acfer 094: The first CM3 chondrite (?). Proceedings, 25th Lunar and Planetary Science Conference. pp.115–116.

Bischoff A. and Schultz L. 2004. Abundance and meaning of regolith breccias among meteorites (abstract). *Meteoritics & Planetary Science* 39:A15.

Bischoff A., Palme H., Schultz L., Weber D., Weber H. W., and Spettel B. 1993. Acfer 182 and paired samples, an iron-rich carbonaceous chondrite: Similarities with ALH 85085 and relationship to CR chondrites. *Geochimica et Cosmochimica Acta* 57:2631–2648.

Bischoff A., Scott E. R. D., Metzler K., and Goodrich C. A. 2006. Nature and origins of meteoritic breccias. In *Meteoritics and the early solar system II*, edited by Lauretta D. S. and McSween H. Y., Jr. Tuscon, Arizona: The University of Arizona Press. pp. 679–712.

Bischoff A., Horstmann M., Pack A., Laubenstein M., and Haberer S. 2010. Asteroid 2008 TC_3—Almahata Sitta: A spectacular breccia containing many different ureilitic and chondritic lithologies. *Meteoritics & Planetary Science* 45:1638–1656.

Brearley A. J. 2003. Nebular versus parent-body processing. In *Meteorites, comets, and planets*, edited by Davis A. Treatise on geochemistry, vol. 1. Amsterdam: Elsevier. pp. 247–268.

Brearley A. J. 2006. The action of water. In *Meteoritics and the early solar system II*, edited by Lauretta D. S. and McSween H. Y., Jr. Tuscon, Arizona: The University of Arizona Press. pp. 587–624.

Brearley A. J. and Papike J. J. 1993. Carbonaceous chondrite clasts in the Kapoeta howardite. Proceedings,

24th Lunar and Planetary Science Conference. pp. 183–184.

Brearley A. J. and Prinz M. 1992. CI chondrite-like clasts in the Nilpena polymict ureilite: Implications for aqueous alteration processes in CI chondrites. *Geochimica et Cosmochimica Acta* 56:1373–1386.

Browning L. B., McSween H. Y., Jr., and Zolensky M. E. 1996. Correlated alteration effects in CM carbonaceous chondrites. *Geochimica et Cosmochimica Acta* 60:2621–2633.

Browning L., McSween H., Jr., and Zolensky M. E. 2000. On the origin of rim textures surrounding anhydrous silicate grains in carbonaceous chondrites. *Meteoritics & Planetary Science* 35:1015–1023.

Bullock E. S., Gounelle M., Lauretta D. S., Grady M., and Russell S. S. 2005. Mineralogy and texture of Fe-Ni sulphides in CI1 chondrites: Clues to the extent of aqueous alteration on the CI1 parent body. *Geochimica et Cosmochimica Acta* 69:2687–2700.

Bunch T. E. and Chang S. 1980. Carbonaceous chondrites—II. Carbonaceous chondrite phyllosilicates and light element geochemistry as indicators of parent body processes and surface conditions. *Geochimica et Cosmochimica Acta* 44:1543–1577.

Ciesla F. J., Lauretta D. S., Cohen B. A., and Hood L. L. 2003. A nebular origin for chondritic fine-grained phyllosilicates. *Science* 299:549–552.

Endress M. and Bischoff A. 1996. Carbonates in CI chondrites: Clues to parent body evolution. *Geochimica et Cosmochimica Acta* 60:489–507.

Endress M., Keil K., Bischoff A., Spettel B., Clayton R. N., and Mayeda T. K. 1994. Origin of dark clasts in the Acfer 059/El Djouf 001 CR2 chondrite. *Meteoritics* 29:26–40.

Gounelle M., Zolensky M. E., Liou J.-C., Bland P. A., and Alard O. 2003. Mineralogy of carbonaceous chondrite microclasts in howardites: Identification of C2 fossil micrometeorites. *Geochimica et Cosmochimica Acta* 67:507–527.

Gounelle M., Engrand C., Alard O., Bland P. A., Zolensky M. E., Russel S., and Duprat J. 2005. Hydrogen isotopic composition of water from fossil micrometeorites in howardites. *Geochimica et Cosmochimica Acta* 69:3431–3443.

Greshake A. 1997. The primitive matrix of the unique carbonaceous chondrite Acfer 094: A TEM study. *Geochimica et Cosmochimica Acta* 61:437–452.

Greshake A., Krot A. N., Meibom A., Weisberg M. K., Zolensky M. E., and Keil K. 2002. Heavily-hydrated lithic clasts in CH chondrites and the related, metal-rich chondrites Queen Alexandra Range 94411 and Hammadah al Hamra 237. *Meteoritics & Planetary Science* 37:281–293.

Grossman J. M., Rubin A. E., and MacPherson G. J. 1988. A unique volatile-poor carbonaceous chondrite with possible implications for nebular fractionation processes. *Earth and planetary Science Letters* 91:33–54.

Hezel D. C. and Palme H. 2010. The chemical relationship between chondrules and matrix and the chondrule matrix complementarity. *Earth and Planetary Science Letters* 294:85–93.

Howard K. T., Benedix G. K., Bland P. A., and Cressey G. 2009. Modal mineralogy of CM2 chondrites by PSD-XRD: Part 1. Total phyllosilicate abundance and the degree of aqueous alteration. *Geochimica et Cosmochimica Acta* 73:4576–4589.

Howard K. T., Benedix G. K., Bland P. A., and Cressey G. 2011. Modal mineralogy of CM chondrites by X-ray diffraction (PSD-XRD): Part 2. Degree, nature and settings of aqueous alteration. *Geochimica et Cosmochimica Acta* 75:2735–2751.

Huss G. R., Rubin A. E., and Grossman J. N. 2006. Thermal metamorphism in chondrites. In *Meteoritics and the early solar system II*, edited by Lauretta D. S. and McSween H. Y, Jr. Tuscon, Arizona: The University of Arizona Press. pp. 567–586.

Jogo K., Krot A. N., and Nagashima K. 2011. Heavily-metamorphosed clasts in the CV carbonaceous chondrite Mokoia: Evidence for strong thermal metamorphism on the CV parent body (abstract #1613). 42nd Lunar and Planetary Science Conference. CD-ROM.

Johnson C. A. and Prinz M. 1993. Carbonate compositions in CM and CI chondrites, and implications for aqueous alteration. *Geochimica et Cosmochimica Acta* 57:2843–2852.

Kallemeyn G. W. and Wasson J. T. 1981. The compositional classification of chondrites—I. The carbonaceous chondrite groups. *Geochimica et Cosmochimica Acta* 45:1217–1230.

Kerridge J. F., MacKay A. L., and Boynton W. V. 1979. Magnetite in CI carbonaceous meteorites: Origin by aqueous activity on a planetesimal surface. *Science* 205:395–397.

Krot A. N., Scott E. R. D., and Zolensky M. E. 1995. Mineralogical and chemical modification of components in CV3 chondrites: Nebular or asteroidal processing? *Meteoritics* 30:748–775.

Lee M. R. and Ellen R. 2008. Aragonite in the Murray (CM2) carbonaceous chondrite: Implications for parent body compaction and aqueous alteration. *Meteoritics & Planetary Science* 43:1219–1231.

Lee M. R. and Smith C. L. 2006. Scanning transmission electron microscopy using a SEM: Applications to mineralogy and petrology. *Mineralogical Magazine* 70:579–590.

Lee M. R., Bland P. A., and Graham G. 2003. Preparation of TEM samples by focused ion beam (FIB) techniques: Applications to the study of clays and phyllosilicates in meteorites. *Mineralogical Magazine* 67:581–592.

Lee M. R., Sofe M. R., and Lindgren P. 2011. Evolution of carbonate mineralization in the CM2 carbonaceous chondrites (abstract #1710). 42nd Lunar and Planetary Science Conference. CD-ROM.

Lindgren P., Lee M. R., Sofe M., and Burchell M. J. 2011. Microstructure of calcite in the CM2 carbonaceous chondrite LON 94101: Implications for deformation history during and/or after aqueous alteration. *Earth and Planetary Science Letters* 306:289–298.

MacPherson G. J., Mittlefehldt D. W., Lipschutz M. E., Clayton R. N., Bullock E. S., Ivanov A. V., Mayeda T. K., and Wang M.-S. 2009. The Kaidun chondrite breccias: Petrology, oxygen isotopes, and trace element abundances. *Geochimica et Cosmochimica Acta* 73:5493–5511.

McSween H. Y., Jr. 1979. Are carbonaceous chondrites primitive or processed? A review. *Reviews of Geophysical Space Physics* 17:1059–1078.

Nakashima D., Nakamura T., and Noguchi T. 2003. Formation history of CI-like phyllosilicate-rich clasts in the Tsukuba meteorite inferred from mineralogy and noble gas signature. *Earth and Planetary Science Letters* 212:321–336.

Newton J., Bischoff A., Arden J. W., Franchi I. A., Geiger T., Greshake A., and Pillinger C. T. 1995. Acfer 094, a uniquely primitive carbonaceous chondrite from the Sahara. *Meteoritics* 30:47–56.

Olsen E. J., Davis A. M., Hutcheon I. D., Clayton R. N., Mayeda T. K., and Grossman L. 1988. Murchison xenoliths. *Geochimica et Cosmochimica Acta* 52:1615–1626.

Petitat M., Marrocchi Y., McKeegan K. D., Mostefaoui S., Meibom A., Zolensky M. E., and Gounelle M. 2011. ^{53}Mn-^{53}Cr ages of Kaidun carbonates. *Meteoritics & Planetary Science* 46:275–283.

Prinz M., Weisberg M. K., Nehru C. E., and Delaney J. S. 1987. EET 83309, a polymict ureilite: Recognition of a new group. 18th Lunar and Planetary Science Conference. p. 802.

Reid A. M., Buchanan P., Zolensky M. E., and Barrett R. A. 1990. The Bholghati howardite: Petrography and mineral chemistry. *Geochimica et Cosmochimica Acta* 54:2161–2166.

Rubin A. E. 2012. Collisional facilitation of aqueous alteration of CM and CV carbonaceous chondrites. *Geochimica et Cosmochimica Acta* 90:181–194.

Rubin A. E. and Wasson J. T. 1986. Chondrules in the Murray CM2 meteorite and compositional differences between CM-CO and ordinary chondrite chondrules. *Geochimica et Cosmochimica Acta* 50:307–315.

Rubin A. E., Trigo-Rodríges J. M., Huber H., and Wasson J. T. 2007. Progressive aqueous alteration of CM carbonaceous chondrites. *Geochimica et Cosmochimica Acta* 71:2361–2382.

Semenko V. P., Bischoff A., Weber I., Perron C., and Girich A. L. 2001. Mineralogy of fine-grained material in the Krymka (LL3.1) chondrite. *Meteoritics & Planetary Science* 36:1067–1085.

Semenko V. P., Jessberger E. K., Chaussidon M., Weber I., Stephan T., and Wies C. 2005. Carbonaceous xenoliths in the Krymka LL3.1 chondrite: Mysteries and established facts. *Geochimica et Cosmochimica Acta* 69: 2165–2182.

Sofe M. R., Lee M. R., and Lindgren P. 2011. Aragonite in the CM carbonaceous chondrites: A proxy for the magnitude of aqueous alteration (abstract #5250). *Meteoritics & Planetary Science* 46:A217.

Tomeoka K. 1990. Phyllosilicate veins in a CI meteorite: Evidence for aqueous alteration on the parent body. *Nature* 345:138–140.

Tyra M. A., Matzel J., Brearley A. J., and Hutcheon I. D. 2010. Variability in carbonate petrography and NanoSims ^{53}Mn/^{53}Cr systematics in paired CM1 chondrites ALH 84051, ALH 84049, and ALH 84034 (abstract #2687). 41st Lunar and Planetary Science Conference. CD-ROM.

Tyra M. A., Brearley A. J., and Guan Y. 2011a. Oxygen isotopic composition of secondary carbonates in CR1 chondrite GRO 95577 (abstract #1639). 42nd Lunar and Planetary Science Conference. CD-ROM.

Tyra M. A., Farquhar J., Guan Y., and Leshin L. A. 2011b. An oxygen isotope dichotomy in CM2 chondritic carbonates—A SIMS approach. *Geochimica et Cosmochimica Acta* 77:383–395.

Wasson T. J. and Rubin A. E. 2009. Composition of matrix in the CR chondrite LAP 02342. *Geochimica et Cosmochimica Acta* 73:1436–1460.

Zolensky M. E. and Ivanov A. 2003. The Kaidun microbreccia meteorite: A harvest from the inner and outer asteroid belt. *Chemie der Erde Geochemistry* 63:185–246.

Zolensky M. E. and McSween H. Y., Jr. 1988. Aqueous alteration. In *Meteorites and the early solar system*, edited by Kerridge J. F. and Matthews M. S. Tuscon, Arizona: The University of Arizona Press. pp. 114–143.

Zolensky M. E., Barrett R. A., and Ivanov A. V. 1991. Mineralogy and matrix composition of clasts in the chondritic breccias Kaidun. 22nd Lunar and Planetary Science Conference. p. 1565.

Zolensky M. E., Barrett R., and Browning L. 1993. Mineralogy and composition of matrix and chondrule rims in carbonaceous chondrites. *Geochimica et Cosmochimica Acta* 57:3123–3148.

Zolensky M. E., Weisberg M. K., Buchanan P. C., and Mittlefehldt D. W. 1996. Carbonaceous chondrite clasts in HED achondrites. Workshop on Evolution of Igneous Asteroids: Focus on Vesta and the HED Meterorites. p. 43.

Zolensky M. E., Mittlefehldt D. W., Lipschutz M. E., Wang M.-S., Clayton R. N., Mayeda T. K., Grady M. M., Pillinger C., and Barber D. 1997. CM chondrites exhibit the complete petrologic range from type 2 to 1. *Geochimica et Cosmochimica Acta* 61:5099–5115.

Zolensky M. E., Nakamura K., Gounelle M., Mikouchi T., Kasama T., Tachikawa O., and Tonui E. 2002. Mineralogy of Tagish Lake: An ungrouped type 2 carbonaceous chondrite. *Meteoritics & Planetary Science* 37:737–761.

Zolensky M. E., Briani G., Gounelle M., Mikouchi T., Ohsumi K., Weisberg M. K., Le L., Satake W., and Kurihara T. 2009. Searching for chips of Kuiper Belt Objects in meteorites (abstract #1288). 40th Lunar and Planetary Science Conference. CD-ROM.

Appendix 1. Compositions of siderite, breunnerite, and dolomite in the carbonate-rich clast (wt% elements).

Carbonate	Na	Mg	Al	Si	S	K	Ca	Cr	Fe	Mn	Ni	Sr	Total
Siderite_1	0.34	9.53	0.01	0.14	0.01	0.01	2.19	0.01	29.03	0.24	0.02	n.d.	41.48
Siderite_2	0.30	9.89	0.02	0.17	0.02	0.01	1.98	0.02	27.07	0.38	0.03	0.01	39.96
Siderite_3	0.26	10.13	0.01	0.15	0.02	0.01	2.20	0.01	26.35	0.39	0.02	n.d.	39.47
Siderite_4	0.31	7.25	0.01	0.13	0.01	0.01	2.70	0.01	30.63	0.29	0.01	n.d.	41.38
Siderite_5	0.32	9.89	n.d.	0.11	n.d.	0.01	2.24	0.02	27.65	0.35	0.02	0.01	40.64
Breunnerite_6 (rim of siderite grain)	0.28	13.21	n.d.	0.11	n.d.	0.01	1.83	0.01	24.03	0.47	0.02	n.d.	39.90

Appendix 1. *Continued*. Compositions of siderite, breunnerite, and dolomite in the carbonate-rich clast (wt% elements).

Carbonate	Na	Mg	Al	Si	S	K	Ca	Cr	Fe	Mn	Ni	Sr	Total
Breunnerite_7 (rim of siderite grain)	0.26	13.95	0.01	0.12	0.01	n.d.	1.59	0.01	21.92	0.32	0.02	n.d.	38.25
Siderite_8	0.40	7.91	0.10	0.60	0.08	0.02	1.64	0.02	28.41	1.03	0.03	n.d.	40.18
Siderite_9	0.41	8.67	n.d.	0.13	n.d.	0.02	1.27	0.01	30.43	0.75	0.02	n.d.	41.74
Siderite_10	0.32	9.34	0.08	0.61	0.07	0.02	1.49	0.01	26.54	0.60	0.05	n.d.	39.06
Dolomite_1	0.12	11.04	n.d.	0.11	0.01	n.d.	22.70	n.d.	3.73	0.33	n.d.	0.04	38.01
Dolomite_2	0.06	9.91	0.01	0.10	0.01	n.d.	23.57	n.d.	3.18	0.05	0.01	0.05	36.99
Dolomite_3	0.08	10.04	n.d.	0.10	n.d.	n.d.	24.27	n.d.	2.92	0.25	0.01	0.06	37.70
Dolomite_4	0.08	10.55	n.d.	0.09	0.01	0.01	22.02	n.d.	4.24	0.18	0.01	0.02	37.20
Dolomite_5	0.08	10.14	0.01	0.11	n.d.	n.d.	22.99	n.d.	2.98	0.24	0.01	0.03	36.58
Dolomite_6	0.12	10.44	n.d.	0.13	n.d.	0.01	23.94	n.d.	3.46	0.21	0.01	0.04	38.32

n.d. = Below detection limits.